

ULTRAVIOLET SPECTROPOLARIMETRY WITH POLSTAR: CONSERVATIVE AND NONCONSERVATIVE MASS TRANSFER IN OB INTERACTING BINARIES

GERALDINE J. PETERS

Department of Physics & Astronomy, University of Southern California, Los Angeles, CA 90089-0484, USA

KEN GAYLEY

Department of Physics & Astronomy, University of Iowa, Iowa City, IA, 52242, USA

RICHARD IGNACE

Department of Physics & Astronomy, East Tennessee State University, Johnson City, TN 37614, USA

CAROL E. JONES

Department of Physics and Astronomy, Western University, London, ON N6A 3K7, Canada

YAËL NAZÉ

GAPHE, University of Liège, Allée du 6 Aout 19c (B5C), 4000-Liège, Belgium

NICOLE ST-LOUIS

Département de physique, Université de Montréal, Campus MIL, 1375 Avenue Thérèse-Lavoie-Roux Montréal (Qc) H2V 0B3

HELOISE STEVANCE

Department of Physics & Astronomy, University of Auckland, 38 Princes Street, 1010, Auckland, New Zealand

JORICK S. VINK

Armagh Observatory and Planetarium, College Hill, BT61 9DG Armagh, Northern Ireland

NOEL D. RICHARDSON

Department of Physics and Astronomy, Embry-Riddle Aeronautical University, 3700 Willow Creek Rd, Prescott, AZ, 86301, USA

JENNIFER L. HOFFMAN

Department of Physics and Astronomy, 2112 E. Wesley Ave., Denver, CO 80208, USA

JAMIE R. LOMAX

Physics Department, United States Naval Academy, 572C Holloway Rd, Annapolis, MD 21402, USA

TOMER SHENAR

Anton Pannekoek Institute for Astronomy and Astrophysics, University of Amsterdam, 1090 GE Amsterdam, The Netherlands

ANDREW G. FULLARD

Department of Physics & Astronomy, Michigan State University, 567 Wilson Rd., East Lansing, MI 48824, MI

PAUL A. SCOWEN

NASA Goddard Space Flight Center, Greenbelt, MD 20771, USA

ABSTRACT

One objective of the *Polstar* spectropolarimetry mission is to characterize the degree of nonconservative mass transfer that occurs at various stages of binary evolution, from the initial mass reversal to the late Algol phase. The proposed instrument combines spectroscopic and polarimetric capabilities, where the spectroscopy can resolve Doppler shifts in UV resonance lines with 10 km/s precision, and polarimetry can resolve linear polarization with 10^{-3} precision or better. The spectroscopy will identify absorption by mass streams seen in projection against the stellar disk as a function of orbital phase, hot accretion spots, as well as scattering from extended splash structures, circumbinary disks, and other flows in and above/below the orbital plane (e.g. *jets*) that fail to be transferred conservatively. The polarimetry affects more the light coming from material not seen against the stellar disk, allowing the geometry of the scattering to be tracked, resolving ambiguities left by the spectroscopy and light-curve information. For example, nonconservative mass streams ejected in the polar direction will produce polarization of the opposite sign from conservative transfer accreting in the orbital plane. Also, time domain coverage over a range of phases of the binary orbit are well supported by the *Polstar* observing strategy. Combining these elements will significantly improve our understanding of the mass transfer process and the amount of mass that can escape from the system, an important channel for changing the final mass, and ultimate supernova, of the large number of massive stars found in binaries at close enough separation to undergo interaction.

1. INTRODUCTION

Most massive stars are born in multiple systems. Spectroscopic surveys in the Tarantula and the Galaxy suggest that between half and two thirds of massive stars undergo binary interactions at some point in their lives (Sana et al. 2012, 2013). Mass transfer is an important step in the evolution of most massive binary systems: it alters the stellar masses, resulting in stripped stars and rejuvenation, which affects the lifetime and death of the stars. As has been called out in the Astro2020 decadal survey, binary interactions are crucial to understand stellar evolution, including the creation of stripped envelope supernovae and kilonovae (Paczynski 1971; Langer 2012; Eldridge et al. 2013; Yoon 2015; Tauris et al. 2017; Laplace et al. 2021), which are key contributors to the chemical evolution of the ISM and provide an important source of feedback. Also, mass lost by a star is not necessarily all accreted by its companion, and escaping mass streams can reduce the final masses of stars by a significant amount that has not been well quantified either observationally or theoretically.

Given the high ionization of massive-star winds, jets, and other circumstellar structures, Thomson scattering

(electron scattering) is expected to dominate the induced polarization, producing a useful sensitivity to the geometry of scattering regions that can be used to resolve ambiguities in the spectroscopic observations. The classic pioneering model by Brown et al. (1978, BME hereafter) approximates the time-varying continuum polarization caused by the illumination of stellar winds in a binary system viewed at an arbitrary inclination angle. In this model, the scattering region is described as an optically thin electron gas. The envelope pattern is assumed to co-rotate with the illumination sources, appropriate for steady-state systems in circular orbit. The illuminators consist of one point source at the center of the scattering region and an additional external point source representing the companion.

Brown et al. (1982) extended the BME model to consider elliptical orbits, and Fox (1994) further extended the formalism to consider finite illuminators. Fox (1994) showed that occultation is only important in very close binary systems, where separation is less than 10 times the radius of the primary star. However, none of these enhancements to the theory included mass streams involved in non-conservative mass transfer. Furthermore,

the time and wavelength dependence of the polarization from escaping mass, which could provide unique constraints and help separate the intrinsic polarization from interstellar polarization (ISP), have not been modeled. However, hints of such polarized signals associated with non-conservative mass transfer have been observed in several systems (e.g. β Lyr, Hoffman et al. 1998; Lomax et al. 2012a) and extending these observations into the UV, the domain of strongest stellar irradiation for hot stars, will help quantify the degree of mass loss.

The optically-thin polarization models are crucial since they provide basic insights into information that continuum polarization can provide. In the case of an axisymmetric envelope around a point source, the observed polarization only depends on three parameters: the optical depth τ of the envelope, the shape of the envelope (described by a single parameter γ defined below), and the inclination i of the symmetry axis relative to the observer. If the envelope is oblate, the observed polarization is parallel to the symmetry axis. Conversely, the observed polarization is perpendicular to the symmetry axis for a prolate envelope. These results are easily understood: for a prolate envelope the density is highest along the poles, and it is these regions—for which the electric vector and hence polarization is perpendicular to the symmetry axis—that will contribute most to the observed flux. This is one of the ways *Polstar's* polarimetric capability can supplement spectroscopic information, helping to describe the mass-transfer structure.

In optically thick envelopes, the simple behavior described above is modified. The orientation is then set not only by where the electric density is highest, it is also set by where the flux escapes. As a consequence it is possible to have the polarization switch sign, and, when the continuous absorption and emissivity is important, the sign can also be wavelength dependent. For an axisymmetric system, the polarization is always perpendicular or parallel to the symmetry axis (since these are the only unique directions). Thus, when there is wavelength dependence in the polarization, a signature of switching from pole-dominated to equator-dominated polarization is a 90 degree rotation in the polarization position angle. By contrast, a switch from intrinsic-dominated to ISM-dominated polarization can be a rotation of the polarization through any position angle. This method is described in more detail in citepAndersson2021.

Line emission offers another probe. For recombination lines it is typically assumed that the emission is unpolarized. Also, some resonance lines are at least partially depolarizing. Consequently line photons, which originate at larger distances in the envelope, will (at least for the optically thin case) show less polarization than the adjacent continuum.

Our view of the mass transfer process in OB interacting binaries was substantially refined with the pioneering high-resolution FUV spectroscopic observations from the *IUE* and *FUSE* spacecraft (<https://archive.stsci.edu/iue/>; <https://archive.stsci.edu/fuse/>). Circumstellar (CS) material was not only in accretions disks, but also in *splash* and other localized outflow regions in the orbital plane, jets that produced mass loss above/below the orbital plane, and high-temperature (10^5 K) plasmas. But inadequate phase coverage within an orbital cycle limited our ability to map these structures and it was difficult to detect outflows above/below the orbital plane (jets) unless the system displayed a total eclipse. Mass loss from the system during the mass transfer phase was difficult to quantify.

In this paper, we consider how the spectroscopic and polarimetric diagnostics of escaping mass streams and circumstellar disks can reveal the fraction of mass that escapes from the system. We begin in Section 2 with a discussion of the brightest systems, expressed in the *r-q diagram*, of greatest importance to the objective of understanding the evolution of mass transfer binaries, which are predominantly B-type systems as they provide a statistically significant sample. Then in Section 3 we lay out the details of the *Polstar* observational scheme, establishing the required observational requirements and connecting them to *Polstar's* projected capabilities, to build confidence in the success of an experiment that combines polarimetry, spectroscopy, and light curve information as a function of orbital phase. Section 4 continues with a discussion of how polarimetry can be used to infer the mass flow structures in interacting binaries, potentially containing disks and jets, given their importance for understanding the conservative and nonconservative elements of the mass transfer budget. This section concludes with an application to the well-known B-type binary β Lyrae from polarimetric data secured from ground-based instrumentation and FUV spectrophotometry from the spacecraft *WUPPE*. Section 5 describes the spectroscopic signatures of mass flow, which crucially complements the polarimetric information because of its quantitative velocity constraints on mass streams, splash zones, high-temperature accretion regions, and plasma jets. Conclusions are given in Section 6.

2. THE INTERACTING BINARY LANDSCAPE

The importance of binarity in the evolution of OB stars and where the Be stars fit into the picture has been discussed since the mid-1970s (Kriz & Harmanec 1975; Plavec & Polidan 1976; Plavec 1976). The fate of a B star depends on how close it is to its nearest neighbor when it reaches the main sequence. If the separation of

the more massive star did not show any obvious evidence of CS material in the *IUE* spectra, an image from the WISE spacecraft (Deschamps et al. 2015) clearly reveals evidence of earlier mass loss.

SV Cen and UX Mon are definitely in the pre-mass reversal phase. SV Cen is distinguished by displaying the fastest known rate of period decrease, ($\dot{P}/P \approx -1.5 \cdot 10^{-5} \text{ yr}^{-1}$, Drechsel & Lorenz 1993). From 1894 to 1993 the period shortened on the average by 2.2 s yr^{-1} , indicating a mass transfer rate of $4 \times 10^{-4} M_{\odot} \text{ yr}^{-1}$. Drechsel et al. (1982) report systemic mass loss in SV Cen from the analysis of *IUE* spectra. UX Mon currently shows a decreasing orbital period of $\dot{P} = -0.260 \text{ s yr}^{-1}$ (Sudar et al. 2011). The primary may be embedded in an optically-thick accretion disk and the system related to the W Serpentis binaries.

All of the Algol binaries shown in Figure 1 were observed with *IUE*. Some observational details are highlighted in Section 5. The mass gainers for all of the Algol binaries plotted in Regions 2 and 3 are rotating supersynchronously, as are about half of the systems in Region 1. This is not a surprise because the gas stream is impacting the gainer’s photosphere with a velocity of about 400 km s^{-1} . It is thought that the systems that are tidally-locked are experiencing a hiatus in the flow in the gas stream. Considering the high velocity of the gas stream, if the impact is tangential one might expect that the material in the flow will head out of the system near phase 0.5 and be lost to the ISM. In fact this is observed: the example of β Lyr, with UV spectropolarimetry from WUPPE (Hoffman et al. 1998; Harmanec et al. 1996), and others discussed in Section 5. Some other objects in Region 2 deserve special mention. CX Dra (Richards et al. 2000) and RY Per (Barai et al. 2004) have similar stellar parameters and periods (6.7-6.9 d) but the former is viewed at an inclination of about 55 deg while the latter displays a total eclipse. This allows us to study mass outflow at two locations in a system residing in Region 2: above/below and in the orbital plane. V356 Sgr is a totally eclipsing system that displays a large optical polarization signature (Lomax et al. 2017a) which is variable. The scatters could be in an extended coplanar circumbinary disk or in a bipolar flow. FUV spectroscopy with the *FUSE* spacecraft (Peters & Polidan 2004) supports the latter. Strong O VI emission that was not eclipsed suggests that a 300 kK plasma resides above/below the orbital plane. Finally V393 Sco (Mennickent et al. 2012) also shows evidence for a bipolar wind. In this case optical line emission that is stronger during eclipse seems to be modulated with phase over its long-period (253 d) photometric cycle. *Polstar*’s polarimetric capabilities are ideal for determining the amount of systemic mass loss above/below the orbital plane.

In the final stages of binary interaction, seen in the

lower left-hand corner of the r - q diagram shown in Figure 1, the five bright Be + sdO (BeS) systems are plotted. These systems are relevant to the current *Polstar* objective $S4$ as providing context for the final stages of a nonconservative transfer process happening earlier, but they are also relevant to another objective, $S3$, which tests the hypothesis that classical Be stars are an intermediate stage of binary mass transfer that eventually produces a BeS system (Jones et al. 2021). The sdO object (cf., Wang et al. 2021, and references therein) are thought to be the stripped down, CNO processed core of the mass loser that transferred significant mass and angular momentum to the Be star. Consider the following scenario. If the mass arrives with too much angular momentum from the orbit of the loser, the mass will need to bleed off some of its extra angular momentum to “condition it” for accretion without overloading the gainer. Recall from discussion above that the component separation and orbital period of mass-transferring binary steadily decreases until the mass ratio is 1.0. After the mass reversal the reverse happens. There appear to be three stages where significant mass and angular momentum loss occurs: During the (near) contact phase (and perhaps a common envelope phase if the stars started out with a large mass difference,) and again as the system passes through Region 2 in the r - q diagram. At other stages the excess angular momentum spins up the gainer (at least its upper envelope and photosphere) and transfers it to a disk structure. As the accretion disk material loses energy due to viscosity it falls to the photosphere, while the angular momentum transported outward by viscosity may contribute to an unstable decretion (mass loss) disk. This continues as the mass loser shrinks below its Roche surface and exposes its core. More information on the sdO object can be found in the *Polstar* objective $S3$ white paper, Jones et al. (2021).

Binary evolution after the BeS stage can take various paths. The sdO object will continue to evolve at a fast rate comparable to what would occur if it were a single star of its original mass, because its core mass reflects its earlier more massive state. Hence it may explode as a core-collapse supernova (CCSNe) and produce a neutron star (ns) or black hole while the gainer is still on the main sequence. This will not unbind the system because of the high mass of the gainer. Then material from the Be star’s disk will fall onto the compact object and produce x-ray emission. As the mass gainer evolves, its radius will approach the dimension of its own Roche surface, significant mass will be transferred back to the compact object, and the x-ray emission will become intense, creating a high mass x-ray binary (HMXRB). Further evolution scenarios are discussed by Postnov & Yungelson (2014), including a possible common envelope

between the evolving gainer and the compact object, which could even lead to a Thorne-Zytkow object (red supergiant with a neutron star at its core) or another sdO star + compact object with an expanding common envelope. The latter could end up as a merger of neutron stars (or black holes) with production of gamma rays and gravitational waves. These are all outcomes that will be altered if the mass transfer is nonconservative, as we wish to observe and characterize.

The spinup of the gainer requires only a small amount of angular momentum, as the lions share is locked up in the binary orbit. Hence angular momentum evolution is related to how stable and conservative is the mass transfer, so we will also track the consequences to binary evolution of total angular momentum loss. For this, we focus on the nonconservative interaction phases alluded to above, and their immediate aftermath, with attention only to the impact on mass loss from the system; the role of angular momentum transport to the gainer is the topic of objective *S3* (Jones et al. 2021).

We assume the mass transfer rate is stabilized by the increasing separation of the stars after $q < 1$, in particular when the L1 point begins to get farther from the donor at $q < 5/6$. If the stars shared a common envelope prior to this (Podsiadlowski 2010), we consider cases where they emerged from that envelope and are now increasing their separation a more rapidly than the growth of the gainer radius r . To guide our interpretation of the possibilities, three theoretical trajectories that curve from upper right to lower left are indicated in Figure 1. The central trajectory assumes complete conservation of both mass and angular momentum (the textbook example), the upper trajectory conserves total mass but loses angular momentum (perhaps from a tiny amount of material escaping an accretion disk at large radius, losing non-negligible angular momentum), and the lower trajectory conserves total angular momentum but loses mass (perhaps from vertical jets induced by energetic “splashes” after the transfer stream collides and deposits its angular momentum).

These three trajectories all assume that at $q = 5/6$ (the canonical point where the Roche lobe around the donor began its expansion as mass was transferred), the r/a ratio was $1/3$, characteristic of type A mass transfer that will ultimately produce a strong depletion of the mass of the donor star and lead to a very low final q . Note that r/a at $q = 5/6$ cannot be much larger than that, or else the gainer would fill its Roche lobe, contrary to the central assumption. The r/a could be smaller than that, so mass-losing trajectories are not the sole path to low r/a values in the figure, but very low r/a values at $q = 5/6$ would be indicative of case C transfer, involving large separations that would be less likely to lead to low final q values and the extreme degrees of

mass transfer most relevant to this objective.

The curves are derived as follows. Assuming circular orbits are maintained, we have that the total angular momentum J obeys at all times

$$J = M_1 M_2 \sqrt{\frac{Ga}{M}}, \quad (1)$$

where M_1 and M_2 are the masses of the gainer and donor respectively, M is the current mass of the system, and a is the current separation between stars. If we assume the gainer is a main-sequence star with radius $r \propto M^{0.6}$, it follows that

$$\frac{r}{a} = \left(\frac{r}{a}\right)_o \left(\frac{q}{q_o}\right)^2 \left(\frac{1+q_o}{1+q}\right)^{4.6} \left(\frac{M}{M_o}\right)^3 \left(\frac{J}{J_o}\right)^{-2} \quad (2)$$

where the subscript o invokes the situation at $q = 5/6$, regarded as the beginning of the stable transfer process when the Roche point begins to move away from the donor (not $q = 1$ because at that point, mass transfer increases a but the Roche point still moves toward the donor so would still induce runaway transfer if conservative). We then assume the simple schematic ansatz that

$$\Delta J = -f_J \Delta J_2 \quad (3)$$

and

$$\Delta M = -f_M \Delta M_1 \quad (4)$$

to allow for loss of total angular momentum J and mass M , as the donor (star 2) gains J_2 and the gainer (star 1) gains M_1 . The result of this ansatz is

$$\frac{r}{a} = \left(\frac{r}{a}\right)_o \left(\frac{q}{q_o}\right)^2 \left(\frac{1+q_o}{1+q}\right)^{3.6} \times \left(\frac{1+q_o+f_M}{1+q+f_M}\right)^3 \left(\frac{1+q_o+f_J}{1+q+f_J}\right)^{-2}. \quad (5)$$

To help interpret this expression, note that $f_M = 1$ implies half the mass being physically transferred from the donor to the gainer is lost in the process, and $f_J = 1$ implies half the angular momentum being gravitationally returned to the donor from the gainer is lost in the process. These values are the representative choices made to produce the curves in Figure 1, where the upper curve uses $f_J = 1$ (and $f_M = 0$) whereas the lower curve uses $f_M = 1$ (and $f_J = 0$). The central curve is fully conservative, so uses $f_J = 0$ and $f_M = 0$.

The way the systems in the figure span a wide range in these parameters suggests that both types of nonconservative evolution might be present, though to what degree is unclear because we do not know the history of the systems, and we do not know what their r/a was at $q = 5/6$. Hence we need observations of the ongoing processes that are capable of discerning the nature of the transfer and losses, to catch it “in the act.”

In particular, we see in the lower left corner a number of systems with very low q and low r/a which, if they evolved conservatively, would track back to very low r/a at mass reversal (or shortly thereafter). This might be difficult to explain, as this is near the peak of r/a , so if r/a was low even there, then the system would need to be a fairly wide binary that could have difficulty transferring enough mass to reach the observed low q . On the other hand, if the r/a was higher, and typical of mass transfer during main sequence evolution (type A), it would be easy to understand how q became so low, but hard to understand how r/a became so low as well, unless the system lost a significant amount of mass (as suggested by the lowest trajectory shown, that of high system mass loss). Such systems could be losing primarily angular momentum rather than mass, such as in decretion at the outer edges of a large disk, thus producing a high lever arm for angular momentum loss.

In contrast, the figure also shows systems with r/a values so high they could not be fit to conservative trajectories, because then they would track back to $r/a > 1/2$ at $q = 1$, and would thus overflow their own Roche lobes. Such high r/a values thus require that the system be losing mass in such a way that does not involve a high loss of angular momentum, possibly in jets perpendicular to the orbital plane. Hence the figure suggests the possibility of both types of mass loss, primarily disklike in some and jetlike in others. Thus we wish to monitor over orbital phase all these systems carefully, both spectrally and polarimetrically, to look for signatures of either geometry of nonconservative mass transfer in the experiment described next.

3. PROPOSED OBSERVING PROGRAM AND TARGET LIST

The *Polstar* observing strategy, instrument requirements, and projected performance is described in this section, as well as the target list that gives sufficient coverage of key systems to achieve the objective denoted *S4*. This objective is to look for spectropolarimetric evidence in currently interacting binaries that can test the hypothesis that mass transfer is significantly nonconservative in its early and rapid phases prior to and shortly following mass reversal. The strategy involves 20 visits (10 for the dimmest targets), mostly spread evenly over the phase of the binary orbit but with a few extra visits over the eclipse phase for those systems that do eclipse. The plan is to combine spectroscopic searches to resolve absorption lines from mass streams seen in projection against the face of the primary gainer, with polarimetric data capable of exposing the presence of free-electron scattering well away from the face of the star. In this way, both the mass transfer rate can be characterized (spectroscopically), as well as the rate of escaping mass

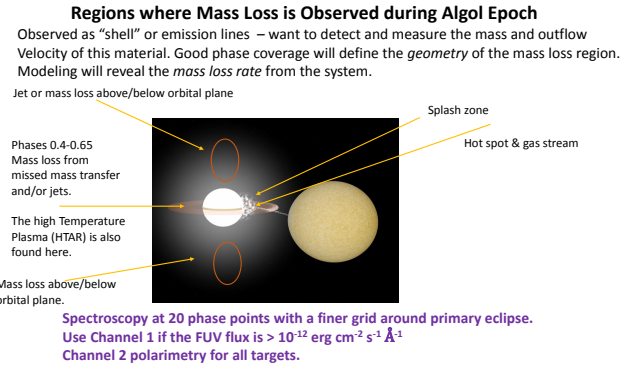


Figure 2. Circumstellar gas/plasma structures observed in Algol-type binaries inferred from phase-dependent FUV spectral lines and polarimetric signatures. The representative system shown is RY Per, from an illustration by Rob Hynes based upon the study of Barai et al. (2004).

(polarimetrically).

Figure 2 shows the locations of the most commonly observed CS structures in mass transfer binaries of the Algol type. The disk parameters are usually determined from modeling Hydrogen emission lines (mostly $H\alpha$). But all of the other structures have been identified from modeling FUV absorption spectra from *IUE*, *FUSE*, or *HST*. These structures include the gas stream, a hot spot at the impact site, a *splash* plasma, mass outflow near phase 0.5 (superior conjunction of the mass losing star), jets, and a high-temperature plasma in the equatorial region at downstream from the impact location.

To carry out the test in this objective, the spectroscopy must be of high enough resolution to pick out mass streams at speeds of a few hundred km s^{-1} , given that the projection toward our line of sight might be less than this, and to put many datapoints across the profiles to diagnose their shape. Opacity in key resonance lines such as C IV at 155 nm and N V at 124 nm is high, as the strength of the resonance compensates for low abundance. Hence if ~ 10 datapoints can be placed across the transient absorption profile that appears at cyclically repeating orbital phase, requiring a resolution of some $R \cong 30,000$, the nature of the mass transfer stream can be deduced spectroscopically. Since the mass transfer rate is high and the infalling velocity gradient is weak, strong UV resonance lines in the stream will be optically thick. But since the Roche lobe overflow region is expected to be rather compact, the stream may not cover a large fraction of the face of the mass gainer, as Fig. (1) shows that the gainer may fill a significant fraction of the interbinary separation. Relatively high SNR $> 50 - 100$ is therefore expected to be required to quantify the highly unsaturated depth of the absorption by the mass stream in each $\cong 10 \text{ km s}^{-1}$ resolution element, when it is caught in projection against the stellar disk. To assist with this desired geometry,

high inclination (often eclipsing) systems are chosen in the target list. In all, the instrument requirements to carry out the spectroscopy of objective S_4 are set at $R = 30,000$ and $S/N = 50 - 100$.

Also, the required polarization precision is set at 1×10^{-3} , with the expectation that nonconservative mass transfer will be indicated by a highly asymmetric geometry of escaping mass. The systems from Fig. (1) that exhibit surprisingly wide separations may require an excess of mass loss over angular momentum loss to achieve such wide separations (as suggested by the dashed curve labeled $d = 0.5$), and so these systems could be expected to exhibit mass loss from the system in polar directions, as shown in Fig. (2). Polarization with a position angle aligned with the orbital plane can be anticipated from these systems if the S_4 hypothesis is correct.

Conversely, systems from Fig. (1) that exhibit surprisingly small separations may require an excess angular momentum relative to mass loss, to cause the orbit to spiral inward suitably to explain their position in this r-q diagram (as suggested by the dashed curve labeled $d = -0.3$). These latter systems could be expected to exhibit mass loss from the system in the equatorial plane, seen spectroscopically as blueshifted “shell” lines at orbital phases where they cross the stellar disk, and associated with a polarization position angle that is perpendicular to the plane of the orbit.

Since the optical depth of the free-electron scattering responsible for this continuum polarization is significantly less than the optical depth in strong UV resonance lines, yet the mass flux of significantly nonconservative transfer would rival that of the mass transfer rate, the free-electron optical depth is expected to be substantial, comparable to free-electron optical depths (~ 0.1) in the strongest O-star winds. Still, The magnitude of such highly aspherical mass concentrations is typically an order of magnitude less than their optical depth to free-electron scattering, and could be further reduced if the streams are concentrated into a narrow solid angle. Hence, we set the required polarization precision necessary to detect these escaping mass streams at 1×10^{-3} .

To establish that the projected performance of the *Polstar* experiment can meet these requirements, the target list in Table (1) shows the required exposure times for each visit, and the number of visits planned, to achieve the indicated SNR. The strategy for the indicated polarization precision involves combining each Ch1 exposure with a Ch2 exposure of half the indicated Ch1 exposure time. This takes advantage of the fact that Ch2 has a roughly factor 3 advantage in effective area over Ch1, such that if the Ch2 stellar flux (characterized near 250 nm instead of the 150 nm characteristic of the UV resonance lines targeted by Ch1) is similar to

the Ch1 flux (as indicated in the flux column in Table 1), a factor 2.5 increase in photon count is achieved by only a factor 1.5 increase in total exposure time per visit. This is deemed a useful strategy for helping to build the stringent polarization precision desired, and is included in the calculation of the indicated polarization precision in the final column. We see from the table that the instrument requirements are met with margin by these projected performance benchmarks. The total observing time implicit in the described observing strategy is 27 days, an acceptable resource allocation for one of twelve objectives in a 3-year mission timeline, while still accounting for a 50% duty cycle, as well as potential time set aside for guest observing.

4. POLARIMETRY OF INTERACTING BINARIES WITH DISKS

4.1. Basics of polarimetric behavior

The *Polstar* team possesses access to a suite of modeling tools, such as Monte Carlo radiative transfer (Whitney et al. 2017; Carciofi et al. 2017; Shrestha et al. 2018), for evaluating polarization from binaries in optically thin or thick regimes. It is however useful to explore the thin scattering regime, particularly the theory advanced by Brown et al. (1978). While thin scattering can be limited in providing quantitatively accurate results Wood et al. (e.g., 1996), it can often provide appropriate order of magnitude results and especially insights into qualitative behavior. Moreover, owing to the low value of the Thomson scattering cross-section, there are many applications in which thin scattering applies at the densities representative of some circumstellar media.

Here we review the Brown et al. (1978) approach for a binary system using somewhat modified notation and presentation that draws partly on Brown et al. (1978) and partly on Brown et al. (1982). The Brown et al. (1978) approaches makes several simplifying assumptions such as point source illumination, neglect of occultation effects, no reflections off either star, and thin scattering as already noted. The authors then proceed to define distributions of the scattering envelope as weighted essentially by lower-term spherical harmonics (e.g., Simmons 1982, 1983). There are 3 broad classifications of these moments: overall asphericity, left-right asymmetry, and front-back asymmetry. Overall asphericity is in relation to the orbital plane of the binary; left-right is respect to the line-of-centers (LOC) joining the two stellar components; and back-front is with respect to each star.

As an example, consider the representative schematics of Figure 3. Top shows a single isotropic point source with a circumstellar disk. This is aspherical and yields a net polarization when the disk is spatially unresolved.

Table 1. Target List

HD Number	Star Name	Spectral Types	System Type*	Period (days)	UV Flux ($\text{erg cm}^{-2} \text{s}^{-1} \text{\AA}^{-1}$) (Channel)	Exp. Time Ch 1 (s)	Number of Phases	SNR	Precision Ch 2 (10^{-3})
5679	U Cep	B8Ve + G8IV	A	2.493	1.00×10^{-11} (1) 1.20×10^{-11} (2)	5000	20	100	0.5
10516	ϕ Per	B1.5e + sdO	BeS	126.673	1.50×10^{-09} (1) 1.50×10^{-09} (2)	600	20	400	0.3
17034	RY Per	B3Ve + F7II-III	A	6.864	4.00×10^{-12} (1) 3.00×10^{-12} (2)	6000	10	70	0.7
19356	Algol	B8V + K2IV	A	2.867	3.00×10^{-09} (1) 3.00×10^{-09} (2)	600	20	600	0.2
33088	TT Aur	B2V + B4IV	EC	1.333	1.00×10^{-11} (1) 5.00×10^{-12} (2)	3000	20	80	0.9
33357	SX Aur	B1.5V + B3V	EC	1.210	2.00×10^{-11} (1) 6.00×10^{-12} (2)	2500	20	100	0.9
41335	HR 2142	B1.5Ve + sdO	BeS	80.913	4.00×10^{-10} (1) 2.00×10^{-10} (2)	200	20	120	0.6
50846	AU Mon	B3Ve + F8III	A	11.113	1.50×10^{-11} (1) 4.00×10^{-12} (2)	3600	20	100	0.8
58978	FY CMa	B0.5Ve + sdO	BeS	37.257	6.00×10^{-10} (1) 6.00×10^{-10} (2)	600	20	250	0.3
65607	UX Mon	A5Ve + G2III	A	5.904	1.00×10^{-12} (1) 1.00×10^{-12} (2)	30000	10	80	0.6
74307	S Cnc	B9.5V + G8IV	A	9.485	4.00×10^{-12} (1) 4.00×10^{-12} (2)	6000	10	70	0.6
97528	TT Hya	B9.5Ve + K3IV	A	6.953	9.00×10^{-12} (1) 4.00×10^{-12} (2)	4000	10	80	0.7
102552	SV Cen	B1V + B6.5III	EC	1.658	6.00×10^{-12} (1) 4.00×10^{-12} (2)	6000	10	80	0.7
136175	U CrB	B6V + F8III-IV	A	3.452	2.00×10^{-11} (1) 4.00×10^{-12} (2)	2500	20	100	0.7
155550	FV Sco	B4IV + F-G:	A	5.727	1.50×10^{-11} (1) 5.00×10^{-12} (2)	4000	10	100	0.6
161741	V393 Sco	B3V + A:	A	7.713	1.50×10^{-11} (1) 8.00×10^{-12} (2)	4000	10	100	0.7
173787	V356 Sgr	B3V + A2II	A	8.896	4.00×10^{-12} (1) 7.00×10^{-12} (2)	6000	10	70	0.5
174237	CX Dra	B2.5Ve + F5III	A	6.696	2.00×10^{-10} (1) 8.00×10^{-11} (2)	900	20	200	0.5
180939	RS Vul	B5V + G1III	A	4.478	3.00×10^{-11} (1) 1.30×10^{-11} (2)	2000	20	100	0.6
181987	Z Vul	B3V + AIII	A	2.455	2.00×10^{-11} (1) 3.10×10^{-11} (2)	2500	20	100	0.4
200120	59 Cyg	B1Ve + sdO	BeS	28.187	1.10×10^{-09} (1) 1.10×10^{-09} (1)	600	20	350	0.3
200310	60 Cyg	B1Ve + sdO	BeS	146.6	5.00×10^{-10} (1) 1.70×10^{-10} (2)	600	20	200	0.5
232121	SX Cas	B5Ve + K3III	A	36.561	4.00×10^{-13} (1) 1.00×10^{-13} (2)	30000	10	50	1

*A=Algol, BeS=Be+sdO, B= β Lyr, EC = Early-Type Contact, O=O-type system, W=W Ser.

As long as the disk is steady-state (i.e., no change of the axisymmetric structure or optical depth), the polarization is constant. The disk is viewed at some inclination, certainly not pole-on but neither edge-on, and the net polarization would be negative by convention: the net polarization would be oriented with the symmetry axis of the disk.

Allowing for finite stellar size of the star (2nd schematic from top) leads to occultation, which can alter the level of net polarization. Although occultation is not treated by [Brown et al. \(1978\)](#), the topic has been considered by several authors (e.g., [Fox 1991](#)). The effect of a finite sized star induces no time variable polarization as long as the disk is steady. Indeed, even if the star itself is variable, the polarization will remain constant being a ratio of polarized flux to total flux.

In the next schematic (3rd from top), a binary companion is added (referring to it as the secondary, whereas the star with disk is the primary), and the polarization becomes time-dependent and cyclical with orbital phase. Even if the disk is steady-state, both the polarization and position angle (PA) can change as the secondary orbits the primary, owing to the changing orientation of how starlight is scattered into the observer sightline. Relative to the secondary, the disk represents a front-back asymmetry for the scattering distribution, but not left-right asymmetry.

The bottom schematic in [Figure 3](#) is another scenario not treated by [Brown et al. \(1978\)](#) displaying a higher inclination in which the secondary eclipses the disk and, in this case, the primary. This is shown for two reasons. First, several targets for *Polstar* are eclipsing close binaries, eclipses contain a wealth of diagnostic material involving both spectral line and continuum polarization for extracting the geometry of the binary system. Although [Brown et al. \(1978\)](#) only deals with point sources, this last schematic also highlight how in a close binary, one expects accretion and thus an accretion stream. Indeed one may even expect a hot spot on the disk where mass from the stream enters the disk (e.g., [Lomax et al. 2012b](#)). Although the schematic does not include a stream or hot spot, these have two main effects.

First, one can easily imagine that the stream creates a break in left-right symmetry about the LOC between the stars. This introduces a lead/lag effect in the polarized light curve relative to eclipsing light curve. Second, a hot spot will have a spectrum, representing a third source of illumination for scattering by electrons in the ionized envelope. The approach of [Brown et al. \(1978\)](#) allows for any number of illuminating sources to explore such effects, especially wavelength-dependence.

Note that orbital eccentricity can also introduce new effects (e.g., [Brown et al. 1982](#); [Manset & Bastien 2000](#)),

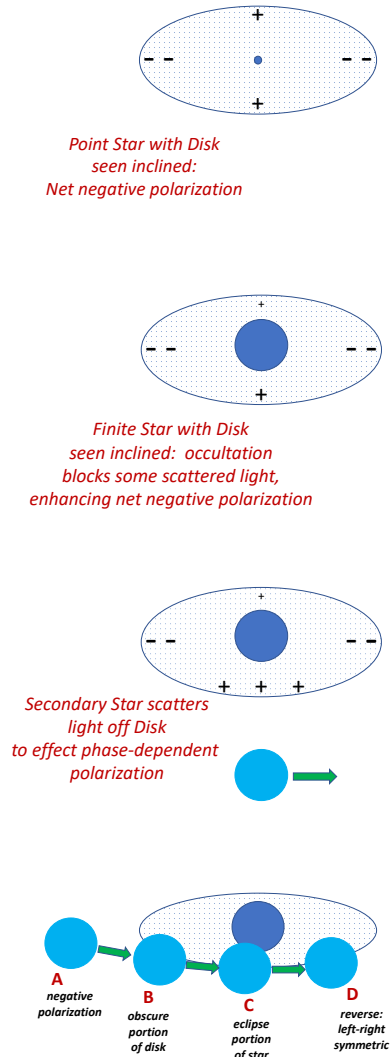


Figure 3. Schematic representation for four scenarios producing constant or time variable linear polarization, as discussed in text. Top is an axisymmetric disk around a point star. Next down is the same disk with a finite sized star. Third is the addition of an orbiting companion star. Bottom is a higher inclination scenario of relevance for many close binary targets of *Polstar* involving eclipse effects.

but for relatively close and typically interacting binaries, we shall assume circular orbits in presenting heuristic models to illustrate (a) how geometry is extracted from variable continuum polarimetry and (b) chromatic effects in the UV that may improve defining the geometry based on the data.

Monte Carlo radiative transfer approaches are capable of taking into account the many realistic factors that influence variable polarization from interacting binaries: the effects of finite stellar size for eclipses and occultation, the effects of multiple scattering, the effects multiple components such as a hot spot or accretion stream.

However, for purposes of illustrating the essentials of modeling polarimetric variability from hot star binaries, and in particular the expectation of chromatic effects in the UV band observable with *Polstar*, an example is developed using the approach of [Brown et al. \(1978\)](#). Following that paper, adopting some notation from [Brown et al. \(1982\)](#), and modifying it slightly, the linear polarization in Stokes-Q and Stokes-U for a binary with a circular orbit is given by

$$q = \bar{\tau} - 3\tau_0 \sin^2 i + G \sin 2i \cos(\phi + \phi_G) - H(1 + \cos^2 i) \cos[2(\phi + \phi_H)] \quad (6)$$

$$u = 2G \sin i \sin(\phi + \phi_G) - 2H \cos i \sin[2(\phi + \phi_H)], \quad (7)$$

where i is the viewing inclination (such that $i = 0^\circ$ is a top-down view of the orbit) and ϕ is the azimuth of the LOC in the orbit plane, relative to the viewer sightline. The coefficients G and H are given in [Brown et al. \(1982\)](#), where G contains terms that are left-right asymmetric, but also top-down asymmetric, while H contains terms that are left-right asymmetric and back-front asymmetric. We will assume that the scattering distribution is top-down symmetric, so $G = 0$. As a result q has a constant term and time or phase dependent term with pattern variation of twice per orbit and potential phase lag signified by ϕ_H . Then u is similar but with no constant term. The polarimetric variation in a $q - u$ diagram is an elliptical figure based on the variable terms, with two circuits about the ellipse in one orbit, and a constant offset in the direction of q . The eccentricity of the ellipse relates to the viewing inclination, with circular for $i = 0^\circ$ and degenerating to a line for $i = 90^\circ$ (since u would be zero).

Definitions for the surviving parameters are:

$$H^2 = \tau_3^2 + \tau_4^2 \quad (8)$$

$$\tan 2\phi_H = \tau_4/\tau_3 \quad (9)$$

$$\bar{\tau} = f_1(\lambda)\bar{\tau}_1 + f_2(\lambda)\bar{\tau}_2 \quad (10)$$

$$\tau_0 = f_1(\lambda)\tau_{01} + f_2(\lambda)\tau_{02} \quad (11)$$

$$\tau_3 = f_1(\lambda)\tau_{31} + f_2(\lambda)\tau_{32} \quad (12)$$

$$\tau_4 = f_1(\lambda)\tau_{41} + f_2(\lambda)\tau_{42}. \quad (13)$$

where f_1 and f_2 are the relative monochromatic luminosities of the respective stars (1 for primary and 2 for secondary) as fractions of the total: $f_1 = L_1/(L_1 + L_2)$ and $f_2 = L_2/(L_1 + L_2)$. As will be addressed shortly, it is these terms that can allow for chromatic effects despite electron scattering being a gray opacity. For the various τ parameters at left, the additional subscript of 1 or 2 for terms on the right signify moment calculations of the scattering distribution relative to the respective

stars. Note that symbol “ τ ” is chosen because those factors scale as optical depths. Each one scales as the product $n_0\sigma_T L$, for n_0 a characteristic number density of electrons, σ_T the Thomson cross-section, and L a characteristic length. And this holds for the various defined components in the system, such as a disk, an accretion stream, a jet, or a wind. The definitions of the τ terms can be found in BME in terms of the integral relations (although those authors refer to shape factors γ , but the integrals are the same).

The offset term involving $\bar{\tau}$ and τ_0 does not contribute to variable polarization. It is an offset, and without additional information, might not be easily disentangled from the ISP, unless the Serkowski fit (e.g., [Taylor et al. 1991](#); [Clayton et al. 1992](#)) is quite well determined. Note that the offset can show chromatic effects in the UV, to be addressed later. It is however the variable polarization that can be straightforwardly attributed to the binary as distinct from the interstellar contribution. Consequently, we ignore the offset in the discussion that follows, although the offset contains additional useful information about the geometry of the stellar system if it can be disentangled from the ISM polarization (e.g., [Nordsieck et al. 2001](#)).

Now to address chromatic effects that have been mentioned several times. The two fractions f_1 and f_2 are wavelength dependent. Since the focus is hot massive stars, in the optical and IR band, the continua spectra of both stars will be approximately Rayleigh-Jeans. As a result, both f_1 and f_2 become constant, as the λ^{-4} factor cancels. Consequently, the polarization is flat across those spectral bands. (The polarization is also flat if one star dominates the luminosity at every wavelength of observation.)

However, in the UV, the two stars will generally have different temperatures and therefore different Wien peaks. The different temperatures and different radii of the stars mean that f_1 and f_2 also become wavelength-dependent, such that the luminosity weighted terms contributing to the q and u produce polarization with chromatic (i.e., not flat polarized spectra). The chromatic effects emphasize certain moment terms more at some wavelength other terms than at other wavelengths, better defining the geometry of the system in relation to model fitting. In particular, it would mean that the phase lead/lag (ϕ_H) is itself chromatic, a strong constraint on geometrical components in the spatially unresolved system. Note that the moment terms expressed as the τ parameters are not chromatic but are fixed by the geometry of the system; it is only the weighted sums that are chromatic by virtue of the two different stellar spectral distributions.

For a simple illustration, [Figure 4](#) shows results using the preceding expressions for a binary involving a

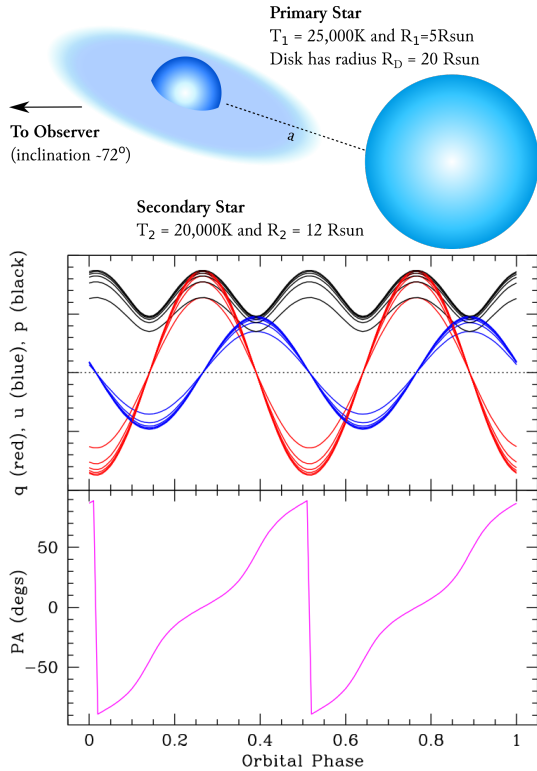


Figure 4. Three panels as illustration of polarimetric variability for a binary system. Top: A cartoon to depict a primary surrounded by an axisymmetric disk orbited by a secondary star with temperatures and sizes indicated. Middle: Variation of q , u , and $p = \sqrt{q^2 + u^2}$ with colors indicated in the label. Note that the different curves are for different wavelength, from 100nm (smallest p) to 400nm (highest p). The variation arises entirely from scattered light by the secondary star, since the disk is axisymmetric about the primary. Bottom: The position angle (PA) change with orbital phase. Note that in this model is no phase lag, for any wavelength, because the system is left-right symmetric; the presence of an accretion stream could change that.

primary star surrounded by an axisymmetric disk; see schematic to scale at top. The primary is hotter and smaller; the secondary is cooler and larger, with parameter values specified in the schematic. The inclination is about 72° ($\cos i = 0.3$). Polarimetric variability is displayed in the middle panel with colors as specified in the label for q , u , and $p = \sqrt{q^2 + u^2}$. Finally at bottom is shown the position angle (PA) variation. Both middle and bottom are plotted with orbital phase, ranging from 0 to 1. At phase zero, the secondary would be forefront if seen edge-on.

Several key points. First the various curves in the middle panel are for different wavelengths of 100nm to 400nm in equal steps. For sake of illustration, the stellar spectra of the two stars are taken as Planckian at the indicated temperatures. For the selected parameters, the lowest polarization is for 100nm, and highest for 400nm. Note how the curves get closer together with increasing wavelength as the individual stars begin to

approach their respective Rayleigh-Jeans spectral distributions, just as expected.

Also, the middle panel has no scale provided. The polarization from thin scattering scales with the optical depth of the medium. We can expect amplitude levels for p at 10^{-4} to 10^{-3} fractional polarizations. But p is positive definite, whereas q and u are signed. For edge-on systems we expect $u = 0$, and q varies between $\pm p$, implying a factor of 2 gain in relative change of polarization, a gain for detection and monitoring purposes.

For the bottom panel, the PA indeed shows cyclic variations at twice rate of the orbital period. This occurs because the geometry is left-right symmetric. However, whereas the polarization curves in the middle panel show chromatic effects, such effects are absent from the PA variation. This is because there is no left-right asymmetry in the geometry - no accretion stream is included in the model. The accretion stream could introduce a phase lag that is wavelength-dependent. What would that look like? At each wavelength the polarization would trace out an ellipse in the $q - u$ diagram. Each ellipse would be of different sizes for different wavelengths, although the eccentricity would remain constant (since the viewing inclination is constant). The effect of different phase would produce relative rotation shifts between the ellipses.

It is important that the approach of BME can be expanded further to include orbital eccentricity (an example being the case of colliding wind systems; REFs) and even a hot spot on the disk. The latter would involve inserting another source of illumination, thus expanding the diversity of chromatic responses. The hot spot will not lie on the LOC of the binary stars, and so would introduce yet an additional phase lag.

The use of BME serves to motivate the fact that the UV spectral band is ideal for extracting important information about the geometry of the system, such as symmetry of the disk, or presence of an accretion stream. When used in conjunction with line profile variability, plus the system light curve (most of our targets are eclipsing variables), the scope of the dataset is rich indeed for extracting densities and kinematics of flows, particularly accretion rates, in the system, and additional component representing non-conservative mass-transfer. While BME neglects radiative transfer effects (such as multiple scattering), our team possesses the expertise to model such effects, guided by BME for qualitative behavior and as benchmarks for the detailed codes in the optically thin limit. For example, [Hoffman et al. \(2003\)](#) applied MCRT methods to explore the effects of multiple scattering in binary systems that include both interior and exterior disk illumination.

While many of the targets are eclipsing binaries, some are not, and polarimetry can provide a measure (or an

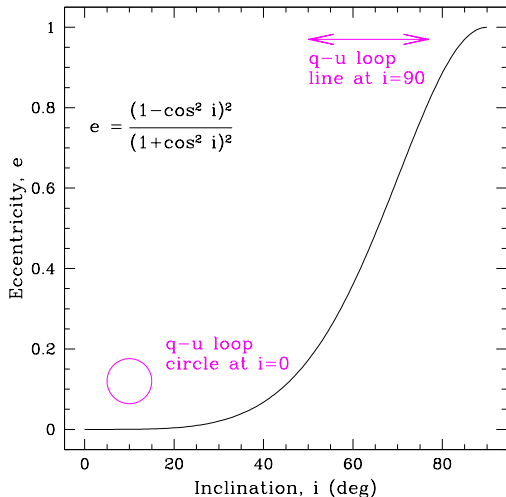


Figure 5. Eccentricity, e , for the elliptical variations in a $q-u$ diagram for a binary in a circular orbit plotted against viewing inclination, i .

additional constraint) to the viewing inclination of the binary orbit. This is important since inclination can often be the greatest ambiguity in the determination of the individual stellar masses. For elliptical variations, the major and minor axes are set by the extrema Δq and Δu , with $e = 1 - (\Delta u^2 / \Delta q^2)$. In relation to the viewing inclination:

$$e = \left(\frac{1 - \cos^2 i}{1 + \cos^2 i} \right)^2. \quad (14)$$

This relationship is plotted in Figure 5. Note that error on the measured eccentricity will depend on $\Delta q / \sigma_q$ and $\Delta u / \sigma_u$, for σ_q and σ_u the polarization precision. At high inclination near edge-on, the effort is aided by the fact that the system will be eclipsing. At low inclination, the challenge is the curve is relatively flat below $i \approx 30^\circ$. For fixed measurement uncertainty, the polarimetric variations must be relatively large to distinguish between a $q-u$ loop that is strictly circular (corresponding to pole-on) and one that is only mildly eccentric. Between about 30° to 80° , the relation is more linear.

4.2. Observable signatures of mass loss

UV polarimetry has proven instrumental in detecting the signatures of mass loss from massive interacting binary systems. In the canonical Algol system β Lyr, Hoffman et al. (1998) showed that the near-UV continuum is polarized at 90° to the optical continuum, indicating that two orthogonal scattering regions exist in the system. These authors hypothesized that the PA rotation across the Balmer jump occurs because UV light is preferentially absorbed by the thick disk, so is only seen when it scatters in a perpendicular bipolar flow (Figure 6). This picture was confirmed by interferometric

observations (Harmanec et al. 1996; Zhao et al. 2008). By contrast, the similar interacting binary V356 Sgr showed no significant PA difference between the optical and the near-UV (Lomax et al. 2017b). This suggests that these Roche-lobe filling binary systems can take on a diversity of geometrical structures, and that using an instrument such as Polstar to characterize a broader sample of these objects will allow deeper insights into their physical nature and evolutionary history.

Lomax et al. (2012a) used multiwavelength polarimetry to constrain the location and extent of the hot spot on the disk edge in β Lyr; extending this analysis into the UV would provide additional 3-dimensional information about the location of hot gas in this and similar systems. In particular, the light curve of β Lyr is known to be strongly wavelength-dependent, with significant eclipse reversals at shorter wavelengths (Kondo et al. 1994; Ignace et al. 2008), suggesting that time-dependent polarimetric monitoring will open a new, heretofore unexplored window into this and similar systems.

Several of the emission lines in β Lyr show polarization position angles that agree with the UV continuum, suggesting that they scatter primarily from the jet or outflow (Hoffman et al. 1998). In the colliding-wind binary system V444 Cyg, the polarized emission lines probe the stratified layers of the WN star’s wind and correlate strongly with the wind geometry as inferred from X-ray emission (Lomax et al. 2015). These findings suggest that the time-dependent line polarization data obtained by Polstar will provide detailed information about the structure of the winds in our massive binary targets.

5. SPECTROSCOPIC SIGNATURES OF CIRCUMSTELLAR PLASMA STRUCTURES IN THE FUV

Circumstellar and photospheric structures that have been identified from FUV spectra are shown in Figure 2 and include the gas stream, hot accretion spot, splash plasma, mass loss at phase 0.5 (superior conjunction of the mass loser), jets (mass loss above/below the orbital plane), and a high-temperature plasma (Peters 2001; Peters & Polidan 2004).

The gas streams in Algol systems are usually detected from *additional* red-shifted absorption in the moderate-ionization species (e.g. Si II, III, IV, S II, III, Al II, III, Mg II) in the orbital phase interval $0.70 < \phi_o < 0.95$, while enhancements in the mass loss are generally seen from violet-shifted absorption in the Si IV wind lines. An example of gas stream absorption is given in Figure 7. Gas stream signatures can appear either as discrete absorption or an *inverse* wind feature.

Recall that if the system is located in *Region 1* of the

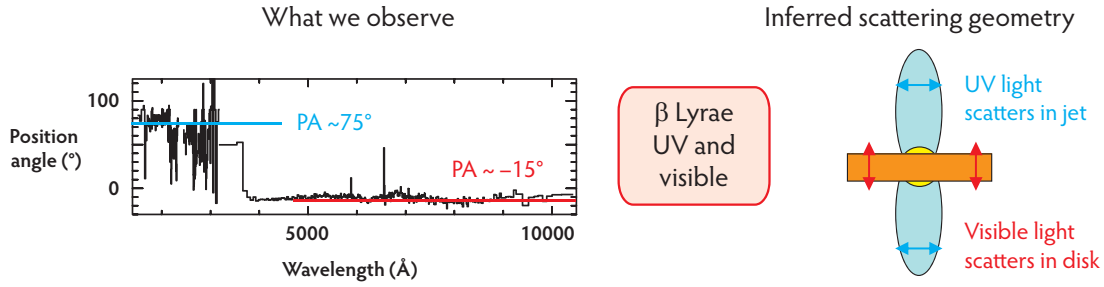


Figure 6. Polarized spectrum (*left*) of β Lyr and interpretive picture (*right*), based on the study by Hoffman et al. (1998). The 90° position angle flip between the near-UV and optical continuum provided key evidence for a jet or outflow in the system oriented orthogonal to the thick accretion disk.

r - q diagram, the mass gainer will present a large enough cross-section that the gas stream will directly impact its photosphere. Since the impact velocity is $\sim 400 \text{ km s}^{-1}$, one expects some degree of shock heating at the impact site. Observations of the direct impact system U Cep ($P=2^{\text{d}}.49$) during the lifetime of the *FUSE* spacecraft present convincing evidence for an accretion hot spot (Peters 2007). In Figure 8 we show an apparent hot spot rotating into, then out of our line-of-sight. Photometric timing allows one to determine the longitude and size of the hot spot. We estimate that the hot spot is located at the substellar point associated with $0^{\text{p}}.90$, covers about 2% of the facing photosphere, and has a temperature of $\sim 30 \text{ kK}$ which is about three times the T_{eff} of the mass gainer. We plan to look for an elevated FUV flux versus phase in the other *Polstar* targets listed in Table 1 to identify/map hot impact regions in other Algols. The role of hot accretion spots in binary star evolution is discussed by van Rensbergen et al. (2008, 2010) who concluded that such spots can help drive mass out of the system and significantly affect the final products of the mass transfer. A likely place to find this type of mass loss would be above/below the orbital plane.

Associated with the accretion spot in U Cep is a localized CS plasma that hovers over the impact region. It

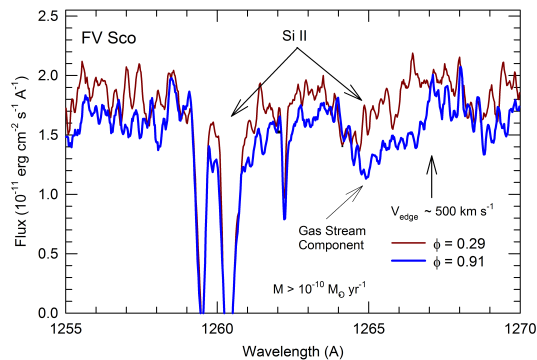


Figure 7. The Si II resonance lines at 126 nm observed at phases 0.91 & 0.29. Note the red-shifted gas stream component at phase 0.91.

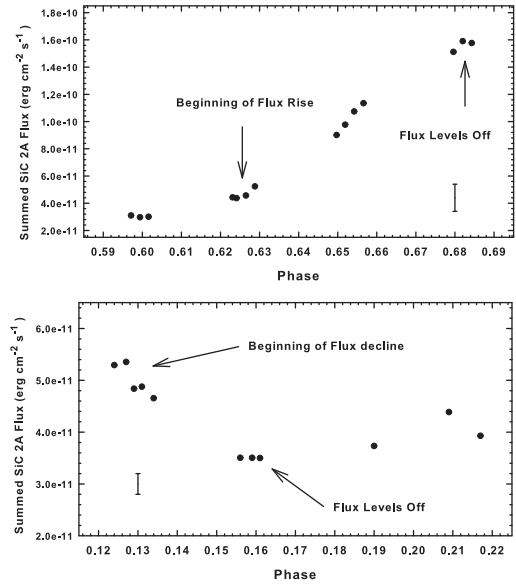


Figure 8. Evidence for a hot accretion spot in U Cep from *FUSE* data. The summed flux from the SiC 2A detector for each exposure obtained on 2004 February 09 and 2007 March 10 is plotted versus phase. In the *upper* panel note that an apparent hot spot rotates into our line-of-sight at phase 0.625 and is fully visible at phase 0.68. In the *lower* panel we observe this hot spot rotating out of our view a half phase later (Peters, et al., in preparation).

is identified from the phase-dependence of the strengths of shell lines of moderate-ionization species. The behavior is shown in Figure 9 in which spectra centered on the Fe III (UV1) resonance multiplet are compared. *Shell-type* absorption features formed in this plasma are observed at phases 0.66, 0.78, and 0.83 but not at phases 0.12, 0.13, and 0.16 even though the hot accretion spot is still visible on the *receding* limb and the FUV flux elevated. Only photospheric lines are observed. When the hot spot is not visible, a pure photospheric spectrum is observed. The localized CS plasma is probably formed as the result of a *splash* associated with the impacting gas stream. The measured velocities of the Fe III shell lines are blue-shifted relative to the photosphere before phase 0.66 but red-shifted in the interval

0.78-0.83. The shell lines from the latter phase interval are apparently formed in the gas stream. Since Fe III and similar species appear to be dominant, the temperature in the plasma is in the range of 20-40 kK. A splash plasma has also been identified in RY Per (Barai et al. 2004). Hot accretion spots and splash plasmas may be commonplace in Algol binaries. Now that we have observational confirmation of their existence, *Polstar* is poised to map out their angular extent and determine how much of the splashed material actually escapes from the system.

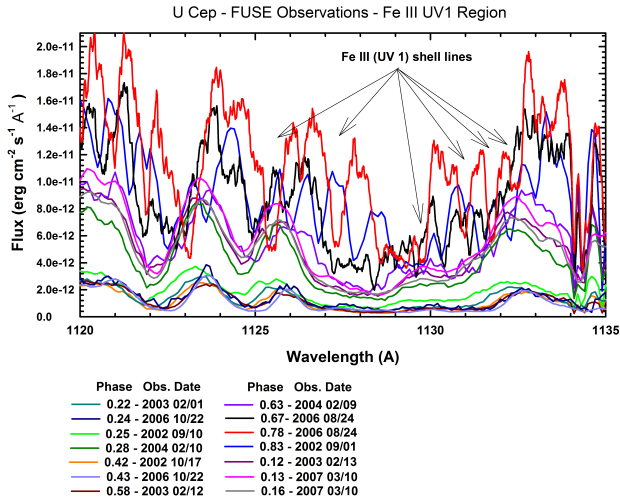


Figure 9. FUSE spectra of U Cep. Note the elevated flux at phases 0.63, 0.67, 0.78, 0.83, 0.12, 0.13, and 0.16. Obvious “shell” structure is observed at phases 0.66, 0.78, and 0.83, but none at the post-conjunction phases even though the hot spot is still visible. The former suggest outflowing plasma from a splash, region while the latter one reveals infall of material from the gas stream (Peters, et al., in preparation).

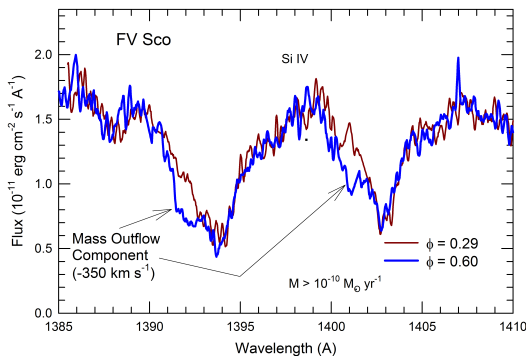


Figure 10. The Si IV resonance lines at 140 nm observed at phases 0.91 & 0.29. Evidence for extensive mass loss at phase 0.60 is seen from a comparison of the Si IV resonance doublet observed at this phase with a similar observation near quadrature.

Optical and UV studies of Algols have revealed that mass loss near $\phi_o \sim 0.5$ is commonplace (Peters (1989, 2001)). Often times it is obvious that the flow is a collimated structure caused by the deflection of the gas stream as it impacts the mass gainer’s photosphere (cf. Figure 10) at a shallow angle. The mass and angular momentum loss from an Algol system are important for theoretical modeling of its evolution, but these quantities, which remains one of the least known, can be modeled from *Polstar* spectroscopic data through spectrum synthesis techniques. Evolution models with nonconservative mass transfer appear to produce better matches to the observed stellar parameters (e.g., van Rensbergen et al. 2008, 2010; Nelson & Eggleton 2001). But this is not a new conclusion. About 40 years ago statistical evidence for *extensive* mass loss during the mass transfer was presented by Giuricin & Mardirossian (1981); Giuricin et al. (1983). These authors considered several conservative and nonconservative studies and concluded that mass and angular momentum loss occurred in 20% of their sample.

Jets, or more generally regions of mass loss above/below the orbital plane may be commonplace in Algol binaries, but they are difficult to detect because most of their material is not along our line-of-sight to the mass gainer. There are both polarimetric (e.g., Hoffman et al. 1998) and FUV spectroscopic (e.g., Peters & Polidan 2004; Plavec 1980) signatures. Noteworthy are emission lines observed during a total eclipse of the mass gainer. These (usually broad) features are from species of moderate-high ionization. Especially interesting are the O VI and N V resonance doublets that indicate plasma temperatures of 300-100 kK.

The discovery of prominent absorption and emission lines of N V, C IV, and Si IV in the UV spectra of Algol-type binaries in the early 1980s with *IUE* revealed the presence of a high temperature component to the circumstellar material (Peters & Polidan 1984; Plavec 1980, 1983). Peters and Polidan called this CS structure the High Temperature Accretion Region (HTAR). They concluded that the HTAR (absorption) lines are formed by resonance scattering in a region of $T_e \sim 10^5$ K, $N_e \sim 10^9$ cm $^{-3}$, and extreme carbon depletion, $C \sim 10^{-3} C_\odot$. The radial velocity behavior of the UV absorption lines provide compelling evidence that the high temperature plasma is associated with the mass gainer. Since the high temperature plasma appears to be enhanced on the *trailing* hemisphere of the primary, it was concluded that the plasma producing the absorption lines is most likely heated as a result of shock heating that occurs as the gas stream impacts either the primary’s photosphere or inner accretion disk. In some of the systems, the material currently being transferred appears to have been processed through the CNO-cycle

in the core of the mass loser. Phase-resolved FUV spectroscopy with *Polstar* will allow us to map the HTAR with more precision and determine if it is an important source of systemic mass loss.

6. SUMMARY

In this white paper we have discussed how we can quantify the amount of systemic mass loss in OB close binaries from FUV polarimetry and high-resolution spectroscopy with *Polstar*. Since 50-100% of the OB stars are formed with one or more companions, stellar evolution calculations for the upper main sequence must consider mass transfer in close binary systems. We have identified three stages of interacting binary evolution that are important epochs of systemic mass and angular momentum loss: just prior to mass reversal and when the system passes through *Region 2* in the r - q diagram before and after reversal. We have identified 23 targets that represent all three regions in the r - q diagram and also have known parameters for their mass gainers and losers as well as the geometry, sizes, and approximate physical conditions in one or more circumstellar structures. With 20 observation pairs (spectroscopy and polarimetry) we will achieve complete phase-coverage with a greater number of observations taking place around the eclipse of the mass gainer where mapping of the asymmetrical CS struc-

tures will be of high precision. In Section 3 we discuss the observing program in detail and show how we can measure the mass flow and loss in the system with *Polstar* with the necessary signal-to-noise and precision that is needed. Combined with the objectives in *S3* (Jones et al. 2021) which will address the binary fraction and angular momentum issues, this project will lead to improved evolutionary tracks for OB stars and a more realistic view of their post-main sequence evolution.

GJP gratefully acknowledges support from NASA grant 80NSSC18K0919 and STScI grants HST-GO-15659.002 and HST-GO-15869.001. She also thanks D. Gies for making the illustration of RY Per by Rob Hynes available to the astronomy community. RI acknowledges funding support from a grant by the National Science Foundation (NSF), AST-2009412. JLH acknowledges support from NSF under award AST-1816944 and from the University of Denver via a 2021 PROF award. Y.N. acknowledges support from the Fonds National de la Recherche Scientifique (Belgium), the European Space Agency (ESA) and the Belgian Federal Science Policy Office (BELSPO) in the framework of the PRODEX Programme (contracts linked to XMM-Newton and Gaia). Scowen acknowledges his financial support by the NASA Goddard Space Flight Center to formulate the mission proposal for *Polstar*.

REFERENCES

- Barai, P., Gies, D. R., Choi, E., et al. 2004, *ApJ*, 608, 989, doi: [10.1086/420875](https://doi.org/10.1086/420875)
- Brown, J. C., Aspin, C., Simmons, J. F. L., & McLean, I. S. 1982, *MNRAS*, 198, 787, doi: [10.1093/mnras/198.3.787](https://doi.org/10.1093/mnras/198.3.787)
- Brown, J. C., McLean, I. S., & Emslie, A. G. 1978, *A&A*, 68, 415
- Carciofi, A. C., Bjorkman, J. E., & Zsargó, J. 2017, in *The Lives and Death-Throes of Massive Stars*, ed. J. J. Eldridge, J. C. Bray, L. A. S. McClelland, & L. Xiao, Vol. 329, 390–390, doi: [10.1017/S1743921317002836](https://doi.org/10.1017/S1743921317002836)
- Clayton, G. C., Anderson, C. M., Magalhaes, A. M., et al. 1992, *ApJL*, 385, L53, doi: [10.1086/186276](https://doi.org/10.1086/186276)
- Deschamps, R., Braun, K., Jorissen, A., et al. 2015, *A&A*, 577, A55, doi: [10.1051/0004-6361/201424772](https://doi.org/10.1051/0004-6361/201424772)
- Drechsel, H., & Lorenz, R. 1993, *Information Bulletin on Variable Stars*, 3868, 1
- Drechsel, H., Rahe, J., Wargau, W., & Wolf, B. 1982, *A&A*, 110, 246
- Eldridge, J. J., Fraser, M., Smartt, S. J., Maund, J. R., & Crockett, R. M. 2013, *Monthly Notices of the Royal Astronomical Society*, 436, 774, doi: [10.1093/mnras/stt1612](https://doi.org/10.1093/mnras/stt1612)
- Fox, G. K. 1991, *ApJ*, 379, 663, doi: [10.1086/170540](https://doi.org/10.1086/170540)
- . 1994, *ApJ*, 435, 372, doi: [10.1086/174819](https://doi.org/10.1086/174819)
- Giuricin, G., & Mardirossian, F. 1981, *ApJS*, 46, 1, doi: [10.1086/190732](https://doi.org/10.1086/190732)
- Giuricin, G., Mardirossian, F., & Mezzetti, M. 1983, *ApJS*, 52, 35, doi: [10.1086/190858](https://doi.org/10.1086/190858)
- Harmanec, P., Morand, F., Bonneau, D., et al. 1996, *A&A*, 312, 879
- Hoffman, J. L., Nordsieck, K. H., & Fox, G. K. 1998, *AJ*, 115, 1576, doi: [10.1086/300274](https://doi.org/10.1086/300274)
- Hoffman, J. L., Whitney, B. A., & Nordsieck, K. H. 2003, *ApJ*, 598, 572, doi: [10.1086/378770](https://doi.org/10.1086/378770)
- Ignace, R., Oskinova, L. M., Waldron, W. L., Hoffman, J. L., & Hamann, W. R. 2008, *A&A*, 477, L37, doi: [10.1051/0004-6361:20078871](https://doi.org/10.1051/0004-6361:20078871)
- Jones, C. E., Labadie-Bartz, J., Nazé, Y., et al. 2021, arXiv e-prints, arXiv:2111.07926. <https://arxiv.org/abs/2111.07926>
- Kondo, Y., McCluskey, G. E., Silvis, J. M. S., et al. 1994, *ApJ*, 421, 787, doi: [10.1086/173691](https://doi.org/10.1086/173691)
- Kriz, S., & Harmanec, P. 1975, *Bulletin of the Astronomical Institutes of Czechoslovakia*, 26, 65
- Langer, N. 2012, *ARA&A*, 50, 107, doi: [10.1146/annurev-astro-081811-125534](https://doi.org/10.1146/annurev-astro-081811-125534)
- Laplace, E., Justham, S., Renzo, M., et al. 2021, arXiv e-prints, arXiv:2102.05036. <https://arxiv.org/abs/2102.05036>
- Linnell, A. P., Peters, G. J., & Polidan, R. S. 1988, *ApJ*, 327, 265, doi: [10.1086/166187](https://doi.org/10.1086/166187)
- Linnell, A. P., & Scheick, X. 1991, *ApJ*, 379, 721, doi: [10.1086/170547](https://doi.org/10.1086/170547)
- Lomax, J. R., Hoffman, J. L., Elias, Nicholas M., I., Bastien, F. A., & Holenstein, B. D. 2012a, *ApJ*, 750, 59, doi: [10.1088/0004-637X/750/1/59](https://doi.org/10.1088/0004-637X/750/1/59)
- . 2012b, *ApJ*, 750, 59, doi: [10.1088/0004-637X/750/1/59](https://doi.org/10.1088/0004-637X/750/1/59)
- Lomax, J. R., Nazé, Y., Hoffman, J. L., et al. 2015, *A&A*, 573, A43, doi: [10.1051/0004-6361/201424468](https://doi.org/10.1051/0004-6361/201424468)

- Lomax, J. R., Fullard, A. G., Malatesta, M. A., et al. 2017a, MNRAS, 464, 1936, doi: [10.1093/mnras/stw2457](https://doi.org/10.1093/mnras/stw2457)
- . 2017b, MNRAS, 464, 1936, doi: [10.1093/mnras/stw2457](https://doi.org/10.1093/mnras/stw2457)
- Lubow, S. H., & Shu, F. H. 1975, ApJ, 198, 383, doi: [10.1086/153614](https://doi.org/10.1086/153614)
- . 1976, ApJL, 207, L53, doi: [10.1086/182177](https://doi.org/10.1086/182177)
- Manset, N., & Bastien, P. 2000, AJ, 120, 413, doi: [10.1086/301439](https://doi.org/10.1086/301439)
- Mennickent, R. E., Kolaczowski, Z., Djurasevic, G., et al. 2012, MNRAS, 427, 607, doi: [10.1111/j.1365-2966.2012.21309.x](https://doi.org/10.1111/j.1365-2966.2012.21309.x)
- Nelson, C. A., & Eggleton, P. P. 2001, ApJ, 552, 664, doi: [10.1086/320560](https://doi.org/10.1086/320560)
- Nordsieck, K. H., Wisniewski, J., Babler, B. L., et al. 2001, in Astronomical Society of the Pacific Conference Series, Vol. 233, P Cygni 2000: 400 Years of Progress, ed. M. de Groot & C. Sterken, 261. <https://arxiv.org/abs/astro-ph/0102073>
- Paczyński, B. 1971, ARA&A, 9, 183, doi: [10.1146/annurev.aa.09.090171.001151](https://doi.org/10.1146/annurev.aa.09.090171.001151)
- Peters, G. J. 1989, SSRv, 50, 9, doi: [10.1007/BF00215915](https://doi.org/10.1007/BF00215915)
- Peters, G. J. 2001, in Astrophysics and Space Science Library, Vol. 264, The Influence of Binaries on Stellar Population Studies, ed. D. Vanbeveren, 79, doi: [10.1007/978-94-015-9723-4_6](https://doi.org/10.1007/978-94-015-9723-4_6)
- Peters, G. J. 2007, in Binary Stars as Critical Tools & Tests in Contemporary Astrophysics, ed. W. I. Hartkopf, P. Harmanec, & E. F. Guinan, Vol. 240, 148–153, doi: [10.1017/S174392130700395X](https://doi.org/10.1017/S174392130700395X)
- Peters, G. J., & Polidan, R. S. 1984, ApJ, 283, 745, doi: [10.1086/162359](https://doi.org/10.1086/162359)
- . 2004, Astronomische Nachrichten, 325, 225, doi: [10.1002/asna.200310224](https://doi.org/10.1002/asna.200310224)
- Plavec, M. 1970, PASP, 82, 957, doi: [10.1086/128996](https://doi.org/10.1086/128996)
- Plavec, M. 1976, in Be and Shell Stars, ed. A. Slettebak, Vol. 70, 439
- Plavec, M., & Polidan, R. S. 1976, in Structure and Evolution of Close Binary Systems, ed. P. Eggleton, S. Mitton, & J. Whelan, Vol. 73, 289
- Plavec, M. J. 1980, in Close Binary Stars: Observations and Interpretation, ed. M. J. Plavec, D. M. Popper, & R. K. Ulrich, Vol. 88, 251–261
- Plavec, M. J. 1983, ApJ, 275, 251, doi: [10.1086/161530](https://doi.org/10.1086/161530)
- Podsiadlowski, P. 2010, NewAR, 54, 39, doi: [10.1016/j.newar.2010.09.023](https://doi.org/10.1016/j.newar.2010.09.023)
- Postnov, K. A., & Yungelson, L. R. 2014, Living Reviews in Relativity, 17, 3, doi: [10.12942/lrr-2014-3](https://doi.org/10.12942/lrr-2014-3)
- Richards, M. T., Koubský, P., Šimon, V., et al. 2000, ApJ, 531, 1003, doi: [10.1086/308491](https://doi.org/10.1086/308491)
- Sana, H., de Mink, S. E., de Koter, A., et al. 2012, Science, 337, 444, doi: [10.1126/science.1223344](https://doi.org/10.1126/science.1223344)
- Sana, H., de Koter, A., de Mink, S. E., et al. 2013, Astronomy & Astrophysics, Volume 550, id.A107, <NUMPAGES>22</NUMPAGES> pp., 550, A107, doi: [10.1051/0004-6361/201219621](https://doi.org/10.1051/0004-6361/201219621)
- Shrestha, M., Neilson, H. R., Hoffman, J. L., & Ignace, R. 2018, MNRAS, 477, 1365, doi: [10.1093/mnras/sty724](https://doi.org/10.1093/mnras/sty724)
- Simmons, J. F. L. 1982, MNRAS, 200, 91, doi: [10.1093/mnras/200.1.91](https://doi.org/10.1093/mnras/200.1.91)
- . 1983, MNRAS, 205, 153, doi: [10.1093/mnras/205.1.153](https://doi.org/10.1093/mnras/205.1.153)
- Sudar, D., Harmanec, P., Lehmann, H., et al. 2011, A&A, 528, A146, doi: [10.1051/0004-6361/201014920](https://doi.org/10.1051/0004-6361/201014920)
- Tauris, T. M., Kramer, M., Freire, P. C. C., et al. 2017, The Astrophysical Journal, 846, 170, doi: [10.3847/1538-4357/aa7e89](https://doi.org/10.3847/1538-4357/aa7e89)
- Taylor, M., Code, A. D., Nordsieck, K. H., et al. 1991, ApJL, 382, L85, doi: [10.1086/186218](https://doi.org/10.1086/186218)
- van Rensbergen, W., De Greve, J. P., De Loore, C., & Mennekens, N. 2008, A&A, 487, 1129, doi: [10.1051/0004-6361:200809943](https://doi.org/10.1051/0004-6361:200809943)
- van Rensbergen, W., De Greve, J. P., Mennekens, N., Jansen, K., & De Loore, C. 2010, A&A, 510, A13, doi: [10.1051/0004-6361/200913272](https://doi.org/10.1051/0004-6361/200913272)
- Wang, L., Gies, D. R., Peters, G. J., et al. 2021, AJ, 161, 248, doi: [10.3847/1538-3881/abf144](https://doi.org/10.3847/1538-3881/abf144)
- Whitney, B. A., Wood, K., Bjorkman, J. E., Cohen, M., & Wolff, M. J. 2017, HO-CHUNK: Radiation Transfer code. <http://ascl.net/1711.013>
- Wood, K., Bjorkman, J. E., Whitney, B. A., & Code, A. D. 1996, ApJ, 461, 828, doi: [10.1086/177105](https://doi.org/10.1086/177105)
- Yoon, S.-C. 2015, Publ. Astron. Soc. Aust., 32, e015, doi: [10.1017/pasa.2015.16](https://doi.org/10.1017/pasa.2015.16)
- Zhao, M., Gies, D., Monnier, J. D., et al. 2008, ApJL, 684, L95, doi: [10.1086/592146](https://doi.org/10.1086/592146)